

The theoretical research of basic function method in incompressible viscous flow and its simulations in three-dimensional aneurysms

SHEN Fang^{1†} & WU WangYi²

¹ State Key Laboratory for Space Weather, Center for Space Science and Applied Research, Chinese Academy of Sciences, Beijing 100190, China;

² State Key Laboratory of Turbulence and Complex Systems & Department of Mechanics and Engineering Science, Peking University, Beijing 100871, China

Basic function method is developed to treat the incompressible viscous flow. Artificial compressibility coefficient, the technique of flux splitting method and the combination of central and upwind schemes are applied to construct the basic function scheme of trigonometric function type for solving three-dimensional incompressible Navier-Stokes equations numerically. To prove the method, flows in finite-length-pipe are calculated, the velocity and pressure distribution of which solved by our method quite coincide with the exact solutions of Poiseuille flow except in the areas of entrance and exit. After the method is proved elementary, the hemodynamics in two- and three-dimensional aneurysms is researched numerically by using the basic function method of trigonometric function type and unstructured grids generation technique. The distributions of velocity, pressure and shear force in steady flow of aneurysms are calculated, and the influence of the shape of the aneurysms on the hemodynamics is studied.

basic function, unstructured grid, aneurysm, viscous incompressible flow, artificial compressibility, flux splitting

Nowadays numerical methods can be mainly classified into two categories: One is to discrete differential operator on structured grids such as the difference method^[1], spectral method^[2], the other is to discrete integral operator on unstructured grids, such as finite element method^[3], finite volume method^[4]. The difference method has been widely used in the field of computational aerodynamics for a long time. And its analytic background was already carefully studied in the past years. The difference method is highly-adaptive, simple and effective. However, it has its own limitations, such as it is difficult to deal with complex boundaries for the coordinate transform, and joined-domain methods should be introduced, and it is also not easy to employ the adaptive remeshing technique in the difference method. Although the finite element method (FEM) has proved its superiority to the difference method in the

aspects described above, FEM will cost much more CPU time and memory than difference method^[5].

To enrich and develop the existing methods, Wu Wangyi proposed a new numerical method: basic function method, and it has been successfully applied to calculate the inviscid compressible flow with good results^[6]. The method directly discretizes differential operator on unstructured grids. We use the expansion of basic function to approach the exact function. A lot of orthogonal and complete families of functions can be used as basic function, for example, polynomial and trigonometric function are in common use, and Legendre polynomial

Received August 24, 2007; accepted December 14, 2008

doi: 10.1007/s11433-009-0118-x

†Corresponding author (email: fshen@spaceweather.ac.cn)

Supported by the National Natural Foundation of China (Grant Nos. 40874077, 40504020, and 40536029) and the National Basic Research Program of China (Grant No. 2006CB806304)

and Chebyshev polynomial also can be selected as basic functions to construct different kinds of basic function schemes. To obtain the values of physical quantities at nodes, the governing equations of differential type are applied for basic function schemes, and the area coordinate or volume coordinate is used for two- or three-dimensional problems. Utilizing the technique of flux splitting and the combination of central and upwind schemes, refs. [6–8] successfully construct the basic function scheme for solving inviscid compressible equations numerically and calculate many one-, two- and three-dimensional typical examples, and the accuracy and resolution of the shock waves are very satisfactory.

In the previous studies of basic function method only inviscid compressible equations are considered. In this paper, the basic function scheme of incompressible viscous flow is developed for the first time. Here we use trigonometric function as basic function because the basic function of trigonometric function type has special advantage in dealing with high-order derivatives, and it remains to have the same order of accuracy for all high-order derivatives. To solve the velocity and pressure synchronously, we introduce Chorin's artificial compressibility technique^[9]. And the volume coordinate is used for three-dimensional problem. The first order basic function of trigonometric function type and the central and upwind schemes for derivatives are constructed successfully. Then we construct the basic function scheme of the trigonometric function type for solving three-dimensional incompressible Navier-Stokes equations numerically for the first time, which adopts the technique of flux splitting method and the combination of central and upwind schemes. Flows in finite-length-pipe and the hemodynamics in two- and three-dimensional aneurysms are studied numerically by using the basic function of trigonometric function type and unstructured grids generation technique. For steady flow, the distributions of velocity, pressure and shear stress in the aneurysms are calculated, and the influence of the shape of the aneurysms on the hemodynamics is studied. Here the unstructured grids are generated by a mixed method formed from advancing front method and Delaunay triangulation method.

1 Generation of the unstructured grids

There are two popular methods to generate the unstructured grids: One is Delaunay triangulation method^[10,11],

which enables to connect the formed points into tetrahedrons by Dirichlet tessellated principle and has virtues of high efficiency and steady generation process; the other is advancing front method^[12,13], which generates surface grid points at first and then takes it as starting front, and moves into interior region. It can generate points automatically through the information provided by background grids and has virtue of controlling the distribution of grid scale, but its generation process is unsteady and efficiency of generation is low.

From above, it can be concluded that advancing front method provides a good way to set points, while Delaunay triangulation is a good point-connecting method. Therefore, based on the above analysis, a new mixing method is proposed by Xie^[7] in three-dimensional problems, which combine the advantage of both methods using advancing front method to set points and Delaunay triangulation to connect points. Similar consideration in two-dimensional problems has been discussed in ref. [14]. We utilize this mixing method to generate the three dimensional unstructured grids in this paper.

2 The basic function of the trigonometric function type

As mentioned above, only trigonometric function is used as basic function in this paper. And the basic function scheme of first-order-precision trigonometric function is studied here emphatically. Comparing with that of high-order-precision, the formula of basic function scheme of first-order-precision is simpler with much less node number, so the CPU time and memory needed are the least.

2.1 Approximation of exact function

We use the expansion of basic function $\phi_i^{(n)}(x, y, z)$ to approach the exact function $f(x, y, z)$:

$$f^{(n)}(x, y, z) = \sum_{i=1}^m f(x_i, y_i, z_i) \phi_i^{(n)}(x, y, z). \quad (1)$$

In the formula above, $f^{(n)}(x, y, z)$ is the n th-order approximation of exact function, $f(x_i, y_i, z_i)$ is the exact value on the node of element. Especially, $f^{(n)}(x, y, z)$ is equal to exact function $f(x, y, z)$ on every node. Any orthogonal and complete family of functions may be used as basic function. The basic function in common use is polynomial^[6,7] and trigonometric function^[10]. When n is equal to different positive integer, different

order approximating function can be obtained, and m is the number of the nodes in elements.

2.2 The central and upwind schemes for derivatives on unstructured grids

In the following parts we will restrict our discussion to basic function of trigonometric function type. In three dimensional problems, in order to make the expression of formula more simple and convenient, volume coordinate is applied.

2.2.1 Introduction of volume coordinates. We define: $L_i = V_i/V$ ($i=1, 2, 3, 4$) as volume coordinate of point P in V . V is the volume of the whole tetrahedral element. V_i is the volume of the tetrahedral element constructed by P and other three vertices (except vertex i).

Obviously, the four volume coordinates L_1, L_2, L_3, L_4 satisfy $L_1 + L_2 + L_3 + L_4 = 1$, so only three of them are independent.

The relationship between L_i and Cartesian coordinates comes as follows:

$$L_i = a_i + b_i x + c_i y + d_i z, \quad (2)$$

where

$$a_i = \frac{1}{6V} \begin{vmatrix} x_j & y_j & z_j \\ x_k & y_k & z_k \\ x_l & y_l & z_l \end{vmatrix}, \quad b_i = -\frac{1}{6V} \begin{vmatrix} 1 & y_j & z_j \\ 1 & y_k & z_k \\ 1 & y_l & z_l \end{vmatrix}, \quad (3)$$

$$c_i = \frac{1}{6V} \begin{vmatrix} 1 & x_j & z_j \\ 1 & x_k & z_k \\ 1 & x_l & z_l \end{vmatrix}, \quad d_i = -\frac{1}{6V} \begin{vmatrix} 1 & x_j & y_j \\ 1 & x_k & y_k \\ 1 & x_l & y_l \end{vmatrix}$$

and V is the tetrahedral volume.

2.2.2 The construction of first order basic function of trigonometric function type and the expression for derivatives. When $n=1$, eq. (1) can be rewritten as

$$f^{(1)}(x, y, z) = \sum_{i=1}^4 f(x_i, y_i, z_i) \phi_i^{(1)}(x, y, z), \quad (4)$$

where $\phi_i^{(1)}(x, y, z)$ is the first order basic function of trigonometric function type. Its expression in volume coordinates is shown as follows:

$$\phi_i^{(1)}(x, y, z) = \frac{1}{2} \left[1 + \sin\left(\frac{\pi}{2} L_i\right) - \cos\left(\frac{\pi}{2} L_i\right) \right] \quad (i=1, 2, 3, 4). \quad (5)$$

The first order derivatives of $f^{(1)}(x, y, z)$ are

$$\frac{\partial f^{(1)}}{\partial X_j} = \sum_{i=1}^4 f(x_i, y_i, z_i) \frac{\partial \phi_i^{(1)}}{\partial X_j}, \quad (X_1 = x, X_2 = y, X_3 = z). \quad (6)$$

Considering eqs. (2) and (5), eq. (6) can be rewritten as

$$\frac{\partial f^{(1)}}{\partial X_j} = \frac{\pi}{4} \sum_{i=1}^4 f(x_i, y_i, z_i) \left[\cos\left(\frac{\pi}{2} L_i\right) + \sin\left(\frac{\pi}{2} L_i\right) \right] B_{ji}, \quad (X_1 = x, X_2 = y, X_3 = z, B_1 = b, B_2 = c, B_3 = d). \quad (7)$$

The second order derivatives of $f^{(1)}(x, y, z)$ can also be deduced as

$$\frac{\partial^2 f^{(1)}}{\partial X_j^2} = \frac{\pi^2}{8} \sum_{i=1}^4 f(x_i, y_i, z_i) \times \left[\cos\left(\frac{\pi}{2} L_i\right) - \sin\left(\frac{\pi}{2} L_i\right) \right] B_{ji}^2. \quad (8)$$

Now let us show how to construct the formulas for derivatives. Due to the need of physical problem, the central scheme and the upwind scheme are introduced.

2.2.3 The first order central scheme (1C). Assume there are N tetrahedral elements around node n , and N

different values of derivative $\left[\frac{\partial^m f}{\partial x^m} \right]_n^{e_i}$ ($i=1, 2, \dots, N$)

on node n can be obtained, e_i stands for the i th tetrahedral element around n . Utilize the weighted

average method to obtain $\left[\frac{\partial^m f}{\partial x^m} \right]_n^{e_i}$ on node n . Because

the less the area of the triangular element, the closer the

value of $\left[\frac{\partial^m f}{\partial x^m} \right]_n^{e_i}$ to the exact value, so it is

appropriate to choose $1/A_{e_i}$ as the weighted coefficient.

Now the first order central scheme of the derivative can be shown as follows:

$$\left[\frac{\partial^m f}{\partial x_j^m} \right]_n^C = \frac{1}{\sum_{i=1}^N \frac{1}{A_{e_i}}} \sum_{i=1}^N \frac{1}{A_{e_i}} \left[\frac{\partial^m f}{\partial x_j^m} \right]_n^{e_i}. \quad (9)$$

2.2.4 The first order upwind scheme (1U). To obtain the upwind scheme for derivative on unstructured grids, the upwind area of triangular element is introduced. We can easily understand the fact in physics: Only the upwind area has its effect on the value of upwind derivative on that node.

Take the two-dimensional region shown in Figure 1 for example. Assume that there are four elements e_i ($i=1, \dots, 4$) in the region. If the upwind direction is parallel to the x -axis, we draw the perpendicular of the x -axis through node the n to split each triangular element around node into upstream region (shadow region) and

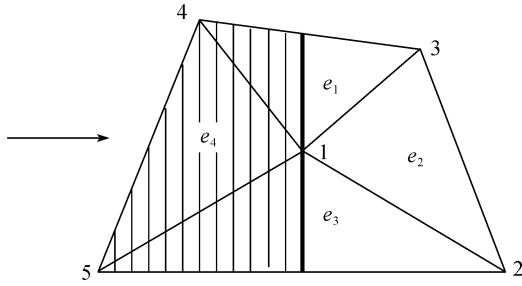


Figure 1

downstream region.

We introduce upwind coefficient $\alpha_n^{e_i}$ on each node of every element. Shown as in Figure 1, for node 1, $\alpha_1^{e_i}$ should be defined as the ratio of shadow region area $A_{e_i,x}$ to the whole area A_{e_i} , that is, $\alpha_1^{e_i} = A_{e_i,x}/A_{e_i}$. In three-dimensional region, upwind coefficient should be the ratio of volumes. Only shadowy area is used to calculate the upwind scheme of derivative.

The first order upwind scheme of the derivative is

$$\left[\frac{\partial^m f}{\partial x_j^m} \right]_n^{U+} = \frac{1}{\sum_{i=1}^N \frac{\alpha_n^{e_i}}{A_{e_i}}} \sum_{i=1}^N \frac{\alpha_n^{e_i}}{A_{e_i}} \left[\frac{\partial^m f}{\partial x_j^m} \right]_n^{e_i} \quad (10)$$

If the downwind area is used to calculate, the first order negative upwind scheme of the derivative could be obtained.

Apparently, if we assign all upwind coefficients $\alpha_1^{e_i}$ with value 1, the upwind scheme (10) will transfer into central scheme (9).

2.2.5 The first order central scheme and upwind scheme of the derivative in three-dimensional unstructured grids. According to the discussion above, we can construct the first order central scheme and upwind scheme of the derivative in three-dimensional unstructured grids.

The first order central scheme and upwind scheme of the m order derivative are

$$\left[\frac{\partial^m f}{\partial x_j^m} \right]_n^{1C} = \frac{1}{\sum_{i=1}^N \frac{1}{A_{e_i}}} \sum_{i=1}^N \frac{1}{A_{e_i}} \left[\frac{\partial^m f^{(1)}}{\partial x_j^m} \right]_n^{e_i} \quad (j=1, 2, 3, x_1 = x, x_1 = y, x_3 = z), \quad (11)$$

$$\left[\frac{\partial^m f}{\partial x_j^m} \right]_n^{1U+} = \frac{1}{\sum_{i=1}^N \frac{\alpha_n^{e_i}}{A_{e_i}}} \sum_{i=1}^N \frac{\alpha_n^{e_i}}{A_{e_i}} \left[\frac{\partial^m f^{(1)}}{\partial x_j^m} \right]_n^{e_i}$$

$$(j=1, 2, 3, x_1 = x, x_1 = y, x_3 = z), \quad (12a)$$

$$\left[\frac{\partial^m f}{\partial x_j^m} \right]_n^{1U-} = \frac{1}{\sum_{i=1}^N \frac{1-\alpha_n^{e_i}}{A_{e_i}}} \sum_{i=1}^N \frac{1-\alpha_n^{e_i}}{A_{e_i}} \left[\frac{\partial^m f^{(1)}}{\partial x_j^m} \right]_n^{e_i}$$

$$(j=1, 2, 3, x_1 = x, x_1 = y, x_3 = z), \quad (12b)$$

where m is equal to 1 or 2 in this paper.

3 The basic function scheme for three-dimensional viscous incompressible Navier-Stokes equations

3.1 Governing equations

The dimensionless Navier-Stokes equations of three-dimensional viscous incompressible flow can be written as follows (the body force is omitted here):

$$\nabla \cdot \mathbf{v} = 0, \quad \frac{\partial \mathbf{v}}{\partial t} + \mathbf{v} \cdot \nabla \mathbf{v} = -\nabla p + \frac{1}{Re} \nabla^2 \mathbf{v} \quad (13)$$

Here L , U_∞ , L/U_∞ and ρU_∞^2 are characteristic length, characteristic velocity, characteristic time and characteristic pressure, respectively. Reynolds number is defined as $Re = \rho U_\infty L / \mu$, and ρ , μ denote density and coefficient of viscosity of the fluid.

Since the velocity doesn't be coupled with the pressure in eq. (13), we introduce artificial compressibility coefficient β into the continuous equation to couple the velocity and pressure which can then be solved synchronously. Therefore, after adoption of the artificial compressibility technique, the dimensionless Navier-Stokes equations can be rewritten as follows:

$$\frac{1}{\beta} \frac{\partial p}{\partial \tau} + \nabla \cdot \mathbf{v} = 0, \quad \frac{\partial \mathbf{v}}{\partial t} + \mathbf{v} \cdot \nabla \mathbf{v} = -\nabla p + \frac{1}{Re} \nabla^2 \mathbf{v}, \quad (14)$$

where τ is virtual time and t is real time, β is the artificial compressibility coefficient. According to the experience before, β gets different values for different flow patterns. There were many reports and discussion in detail about β in ref. [15], for example, the smaller β is, the bigger error is, while the bigger β is, the more poor convergence is, and usually β is between 1 and 10. The values of β in most numerical examples of this paper are taken in the range between 1 and 10.

3.2 Flux splitting method and the expression of basic function scheme

After the viscous incompressible N-S equations are rewritten as hyperbolic equations, eq. (14) can be dealt with using flux splitting technique. According to the feature of the equations, we use first order upwind scheme for inertia terms and use central scheme for viscous terms.

3.2.1 Flux splitting. First, we apply flux splitting technique for N-S equations (14). Eq. (14) can be rewritten as three-dimensional N-S equations of conservative form with artificial compressibility treatment, that is^[16]

$$I_m \frac{\partial Q}{\partial t} + \frac{\partial Q}{\partial \tau} + \frac{\partial(E - E_v)}{\partial x} + \frac{\partial(F - F_v)}{\partial y} + \frac{\partial(G - G_v)}{\partial z} = 0, \quad (15)$$

where $I_m = \text{diag}(0,1,1,1)$ $I_m = \text{diag}(0,1,1,1)$ when flow is unsteady, and $I_m = 0$ when flow is steady.

$$\begin{aligned} Q &= (p, u, v, w)^T, \quad E = (\beta u, u^2 + p, uv, uw)^T, \\ F &= (\beta v, uv, v^2 + p, vw)^T, \quad G = (\beta w, uw, vw, w^2 + p)^T, \\ E_v &= \frac{1}{Re} (0, u_x, v_x, w_x)^T = \frac{\partial H}{\partial x}, \\ F_v &= \frac{1}{Re} (0, u_y, v_y, w_y)^T = \frac{\partial H}{\partial y}, \\ G_v &= \frac{1}{Re} (0, u_z, v_z, w_z)^T = \frac{\partial H}{\partial z}. \end{aligned} \quad (16)$$

Let

$$R = \frac{\partial(E - E_v)}{\partial x} + \frac{\partial(F - F_v)}{\partial y} + \frac{\partial(G - G_v)}{\partial z}, \quad (17)$$

and we have

$$\frac{\partial Q}{\partial \tau} = -R - I_m \frac{\partial Q}{\partial t}. \quad (18)$$

In this paper, we only consider the steady flow, so eq. (18) can be rewritten as

$$\Delta Q = -\Delta \tau \cdot R. \quad (19)$$

And eq. (17) can be rewritten as

$$R = A \frac{\partial Q}{\partial x} + B \frac{\partial Q}{\partial y} + C \frac{\partial Q}{\partial z} - H_{xx} - H_{yy} - H_{zz}, \quad (20)$$

where

$$A = \frac{\partial E}{\partial Q} = \begin{pmatrix} 0 & \beta & 0 & 0 \\ 1 & 2u & 0 & 0 \\ 0 & v & u & 0 \\ 0 & w & 0 & u \end{pmatrix}, \quad B = \frac{\partial F}{\partial Q} = \begin{pmatrix} 0 & 0 & \beta & 0 \\ 0 & v & u & 0 \\ 1 & 0 & 2v & 0 \\ 0 & 0 & w & v \end{pmatrix},$$

$$C = \frac{\partial G}{\partial Q} = \begin{pmatrix} 0 & 0 & 0 & \beta \\ 0 & w & 0 & u \\ 0 & 0 & w & v \\ 1 & 0 & 0 & 2w \end{pmatrix}. \quad (21)$$

We utilize the first order upwind scheme for inertia terms of the first order and the first order central scheme for viscous terms of the second order.

The matrix A can be expressed as $A = R_x A_x R_x^-$, where A_x is the characteristic diagonal matrix. Its expression is $A_x = \text{diag}(\lambda_x^1, \lambda_x^2, \lambda_x^3, \lambda_x^4)$, and the characteristic number can be deduced as follows:

$$\begin{aligned} \lambda_x^1 &= \lambda_x^2 = u, \quad \lambda_x^3 = u + \sqrt{u^2 + \beta}, \\ \lambda_x^4 &= u - \sqrt{u^2 + \beta}, \end{aligned} \quad (22)$$

We split A_x into

$$A_x = A_x^+ + A_x^-, \quad A^\pm = R_x A_x^\pm R_x^-, \quad A = A^+ + A^-, \quad (23)$$

Let $C_x = \sqrt{u^2 + \beta}$, and we have $A = \frac{1}{4C_x(1+u^2/\beta)}$

$\times (a_{ij})$ ($i, j = 1, 2, 3, 4$),

where

$$\begin{aligned} a_{11} &= 2(1+u^2/\beta)C_x(\lambda_3 + \lambda_4) - 2C_x^2 u / \beta(\lambda_3 - \lambda_4), \\ a_{12} &= 2C_x^2(\lambda_3 - \lambda_4), \\ a_{21} &= (1+u\lambda_x^3/\beta)\lambda_3[2(1+u^2/\beta) - 2C_x u / \beta] \\ &\quad + (1+u\lambda_x^4/\beta)\lambda_4[-2(1+u^2/\beta) - 2C_x u / \beta], \\ a_{22} &= 2C_x[(1+u\lambda_x^3/\beta)\lambda_3 + (1+u\lambda_x^4/\beta)\lambda_4], \\ a_{31} &= -4C_x v \lambda_1 / \beta + 2(1+u^2/\beta)v(\lambda_3 \lambda_x^3 - \lambda_4 \lambda_x^4) / \beta \\ &\quad - 2C_x uv(\lambda_3 \lambda_x^3 + \lambda_4 \lambda_x^4) / \beta^2, \\ a_{32} &= -4C_x uv \lambda_1 / \beta + 2C_x v(\lambda_3 \lambda_x^3 + \lambda_4 \lambda_x^4) / \beta, \\ a_{33} &= 4C_x \lambda_1(1+u^2/\beta), \\ a_{41} &= -4C_x \omega \lambda_2 / \beta + 2(1+u^2/\beta)\omega(\lambda_3 \lambda_x^3 - \lambda_4 \lambda_x^4) / \beta \\ &\quad - 2C_x u \omega(\lambda_3 \lambda_x^3 + \lambda_4 \lambda_x^4) / \beta^2, \\ a_{42} &= -4C_x u \omega \lambda_2 / \beta + 2C_x \omega(\lambda_3 \lambda_x^3 + \lambda_4 \lambda_x^4) / \beta, \\ a_{44} &= 4C_x \lambda_2(1+u^2/\beta), \\ a_{13} &= a_{14} = a_{23} = a_{24} = a_{34} = a_{43} = 0. \end{aligned}$$

The matrix B and C also can be split in the same way.

3.2.2 The basic function scheme for viscous incompressible N-S equations. Based on the analysis above, the expression of the first order basic function scheme

for three-dimensional viscous incompressible N-S equations is as follows (explicit scheme):

$$Q^{n+1} = Q^n - \Delta \tau \left\{ \left[A^+ \left(\frac{\partial Q}{\partial x} \right)^{1U+} + B^+ \left(\frac{\partial Q}{\partial y} \right)^{1U+} + C^+ \left(\frac{\partial Q}{\partial z} \right)^{1U+} \right] + \left[A^- \left(\frac{\partial Q}{\partial x} \right)^{1U-} + B^- \left(\frac{\partial Q}{\partial y} \right)^{1U-} + C^- \left(\frac{\partial Q}{\partial z} \right)^{1U-} \right] - \left[\left(\frac{\partial^2 H}{\partial x^2} \right)^{1C} + \left(\frac{\partial^2 H}{\partial y^2} \right)^{1C} + \left(\frac{\partial^2 H}{\partial z^2} \right)^{1C} \right]^n \right\}, \quad (24)$$

where $\left[\frac{\partial^2 H}{\partial x_j^2} \right]^{1C}$ ($j=1, 2, 3, x_1=x, x_2=y, x_3=z$) is

given by eq. (11) ($m=2$), and $\left[\frac{\partial Q}{\partial x_j} \right]^{1U+}, \left[\frac{\partial Q}{\partial x_j} \right]^{1U-}$

are given by eqs. (12a) and (12b) ($m=1$), respectively.

Eq. (24) is the first order basic function scheme of the trigonometric function type for three-dimensional viscous incompressible flow.

The expression of the first order basic function scheme of the trigonometric function type for two-dimensional incompressible flow N-S equations can be deduced in the same way^[5].

4 Numerical examples

Using the basic function scheme of the trigonometric function type for solving three-dimensional incompressible Navier-Stokes equations numerically, flows in finite-length-pipe are calculated first, after the method is proved elementary, the hemodynamics in two- and three-dimensional aneurysms are researched numerically.

Boundary conditions of our examples are

Wall: $u=v=w=0$; entrance: $p=P_0, u=U_0, v=w=0$, exit: $p=0, \partial u/\partial x=0, \partial v/\partial x=0, \partial w/\partial x=0$, where $P_0=9.0 \text{ kPa}$ ^[17].

4.1 Numerical results and analysis of the finite-length pipe

Considering the symmetry of the pipe, we only study the flow pattern on its symmetrical section. The isolines of pressure at the symmetrical section of $z=0$ are shown as in Figure 2(a). Figures 2(b)–(d) depict the velocity distributions near the entrance on sections of $0.1R, 0.7R$

and $4R$ away from the entrance, respectively. Figure 2(e) shows the comparison of the velocity calculated on sections of $x=0, x=\pm 5R$ with that of the Poiseuille flow.

From the figures mentioned above, it can be concluded that the velocity and pressure distributions of the finite-length-pipe calculated by our method are in agreement with the exact solutions of Poiseuille flow at the center and a majority of region, and the velocity distributions near the entrance present the feature of entrance flow^[18]. The three-dimensional incompressible N-S equations we used are intact and are never simplified, the agreement of results calculated by our method with that of the exact solutions of Poiseuille flow illustrates that the basic function method of trigonometric function type is feasible to simulate numerically the viscous incompressible flow.

4.2 Numerical results and analysis of the hemodynamics in the two-dimensional aneurysm

Recently, many numerical simulations about aneurysm were made^[19,20]. For example, Zhang et al.^[19] used an axis-symmetrical model to numerically calculate the pulsatile flow fields in rigid abdominal aortic aneurysm (AAA), in which they applied pulsatile velocity inflow boundary condition as input, and they conducted the simulation with Flunet 6.2. Their results show that there are one or more vortexes in the AAA bulge, and a fairly high wall shear stress exist at the distal end.

The parameters we take in this example are according to ref. [17]. Density and coefficient of viscosity of the blood are taken as $\rho=1000 \text{ kg}\cdot\text{m}^{-3}$ and $\mu=0.0035 \text{ Pa}\cdot\text{s}$, respectively. And $L=40R, R=0.002 \text{ m}$, where L and R denote the length and the radius of blood vessel, respectively. Therefore the influence of entrance and exit on the flow in aneurysm can be ignored. Reynolds number is taken as $Re=\rho U_0 R/\mu=400$.

The velocity vector plot (Figure 3(a)) and the wall shear stress profile vs. arc length in the aneurysm (Figure 3(b)) are calculated for the two-dimensional aneurysm of half-spherical type and the wall shear stress profile (Figure 3(c)) has been compared with that from ref. [19]. The length of the line and the arrowhead in Figure 3(a) denote the size and direction of the velocity vector, respectively. It can be seen that the blood in the tube flows into aneurysm forms a counter-clockwise pattern of recirculation vortex zone in the aneurysm and then flows back to the tube. As seen in Figure 3(b), shear

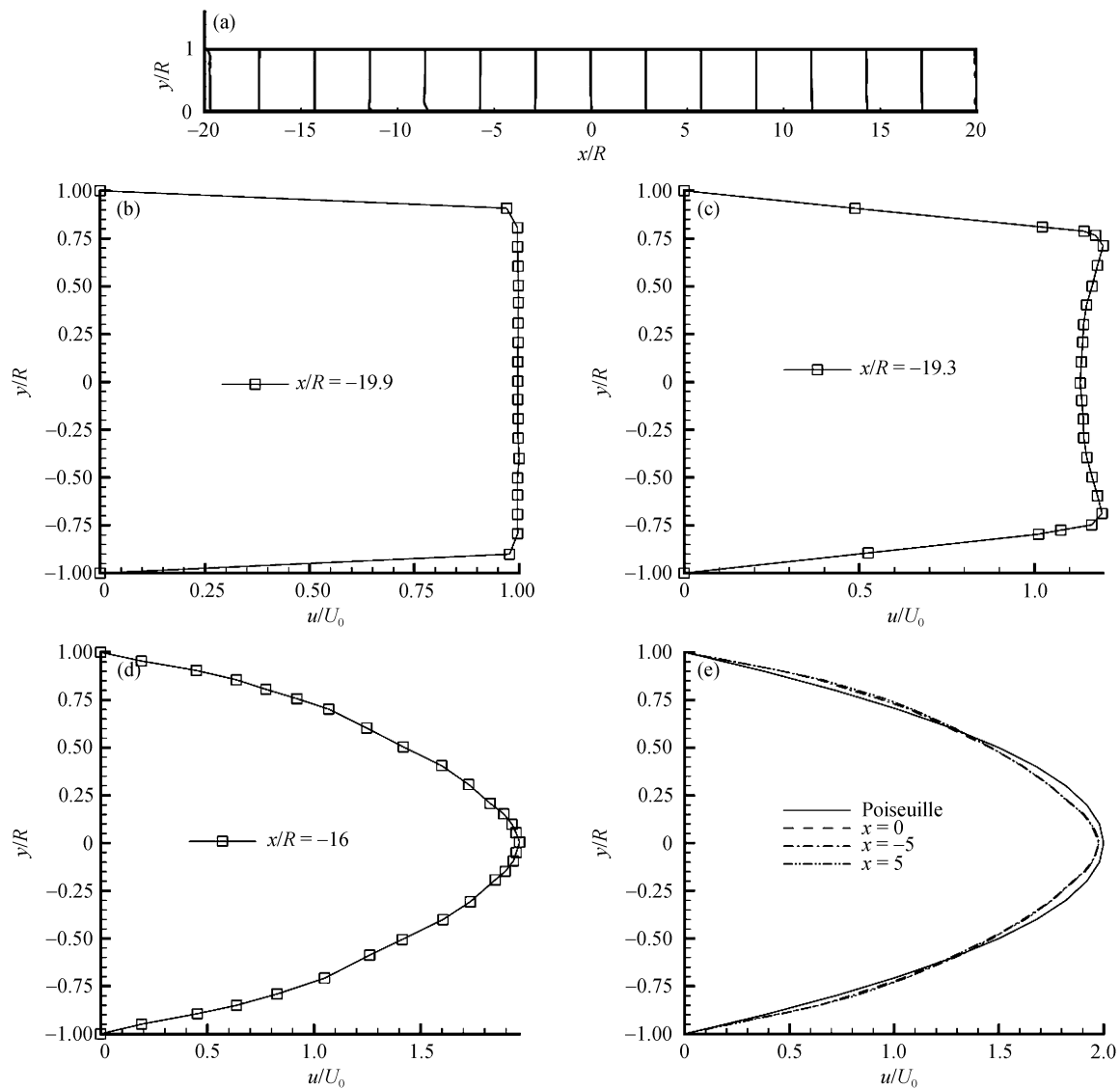


Figure 2 The flows in the finite-length pipe. (a) Isolines of pressure ($z = 0$); (b) velocity distribution of $0.1R$ from the entrance; (c) velocity distribution of $0.7R$ from the entrance; (d) velocity distribution of $4R$ from the entrance; (e) velocity distribution compare among $x = 0$, $x = \pm 5R$ and Poiseuille exact result.

stress in the close and distal region is obvious larger than that in the other region of the aneurysm wall, and the maximal value of the wall shear stress is reached in the distal region. Figure 3(c) gives the shear stress profile from ref. [19] with the same shape as our two-dimensional aneurysm. It can be seen from Figure 3(c) that in the case of Reynolds number 400, the shear stress along the aneurysm wall and its value in the close and distal region are quite close to that in Figure 3(b). The pressures at entrance and exit are not given in ref. [19], so the examples as compared here may not be exactly the same.

4.3 Numerical results and analysis of the hemodynamics in the three-dimensional aneurysm

Two shapes of three-dimensional aneurysms are studied.

And the velocity vector plot, the shear stress profiles and pressure distribution along the wall of aneurysm, and the influence of the shape of the aneurysms on the hemodynamics are numerically researched. The geometric configurations.

The velocity vector plots at the symmetrical section of $z = 0$ obtained from Model 1 and Model 2 are shown in Figures 4(a) and (b), respectively. There are no vortex zones appearing in the aneurysms from Model 1 or Model 2, which is different with the two-dimensional aneurysm^[20].

The shear stress profiles along the wall of aneurysms at the symmetrical section obtained from Model 1 and Model 2 are shown in Figures 4(c) and (d), respectively. The shear stress profiles are similar to that from two-

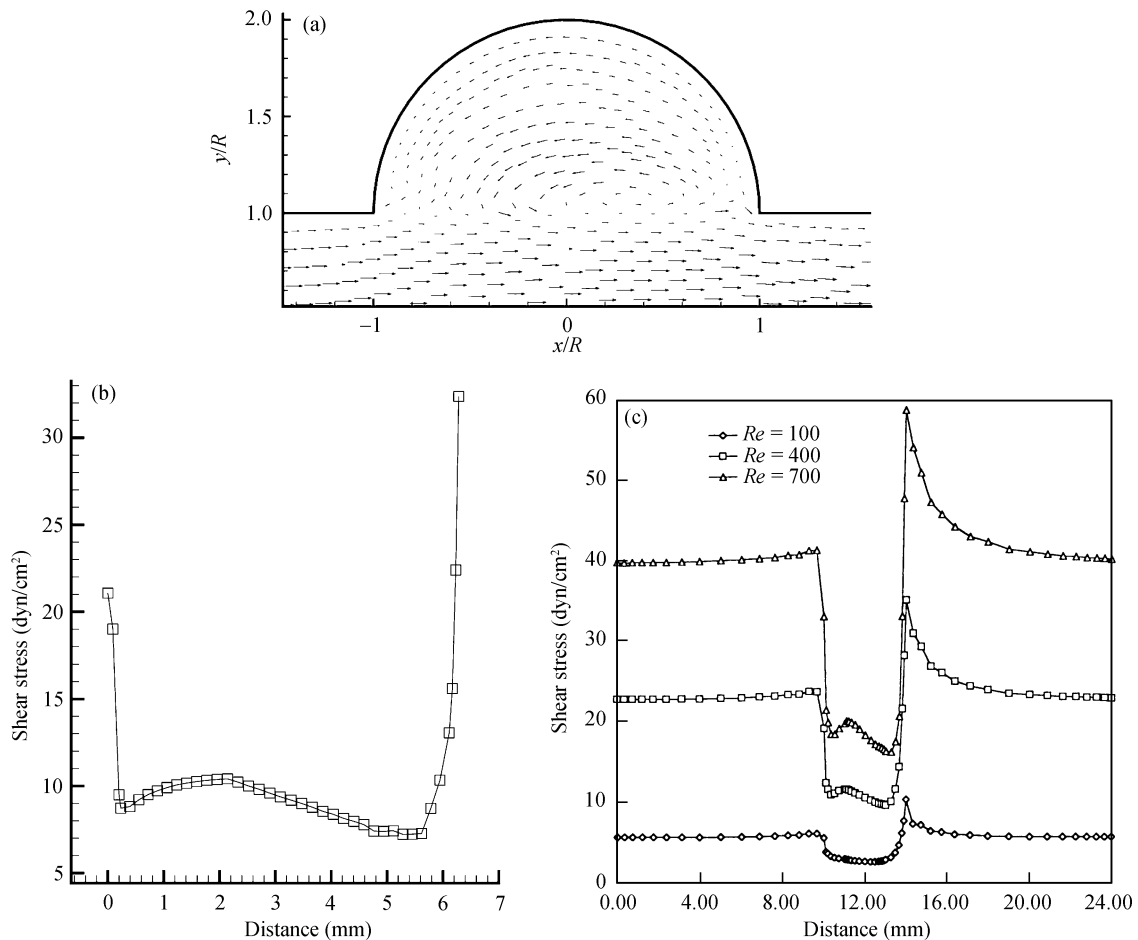


Figure 3 2D half-spherical aneurysm. (a) Velocity vector; (b) the shear stress profiles along the wall of aneurysm; (c) the shear stress profiles along the axis $x=0$ in ref. [19]. $1 \text{ dyn} = 10^{-5} \text{ N}$.

Table 1 Dimensions of three-dimensional aneurysms studied (R , parent artery radius)

Model	Aneurysm shape	Ostium width	Aneurysms radius	Ostium-to-Dome distance
1	half-spherical	$2R$	R	R
2	less-than-half-spherical	$1.6R$	R	$0.4R$

dimensional aneurysms, and the maximal shear stresses all exhibit in the distal region. This maximal level also increases with increasing aneurysm Ostium-to-Dome distance.

The pressure distributions along the wall of aneurysm at the symmetrical sections obtained from Model 1 and Model 2 are shown in Figures 4(e) and (f), respectively. The maximal pressure exhibits near the distal region both in Model 1 and Model 2.

4.4 Conclusions

From the analysis above for two- and three-dimensional

aneurysm, we can conclude that

- 1) The maximal shear stresses and pressures all exhibit in or near the distal region of the aneurysms, so the distal region of the aneurysms is the dangerous region where the aneurysm growth and rupture often happen. This conclusion is also pointed out in refs. [19–22].
- 2) There exists vortex zone in the two-dimensional aneurysms, but no vortex zone appears in the three-dimensional aneurysms, which may be caused by the relatively rough meshes.
- 3) The maximal shear stress on the aneurysms wall will increase with increasing aneurysms size at fixed Reynolds number ($Re=400$).
- 4) However, further studies should consider pulsatile velocity inflow boundary condition as input (ref. [19]), and much denser meshes.

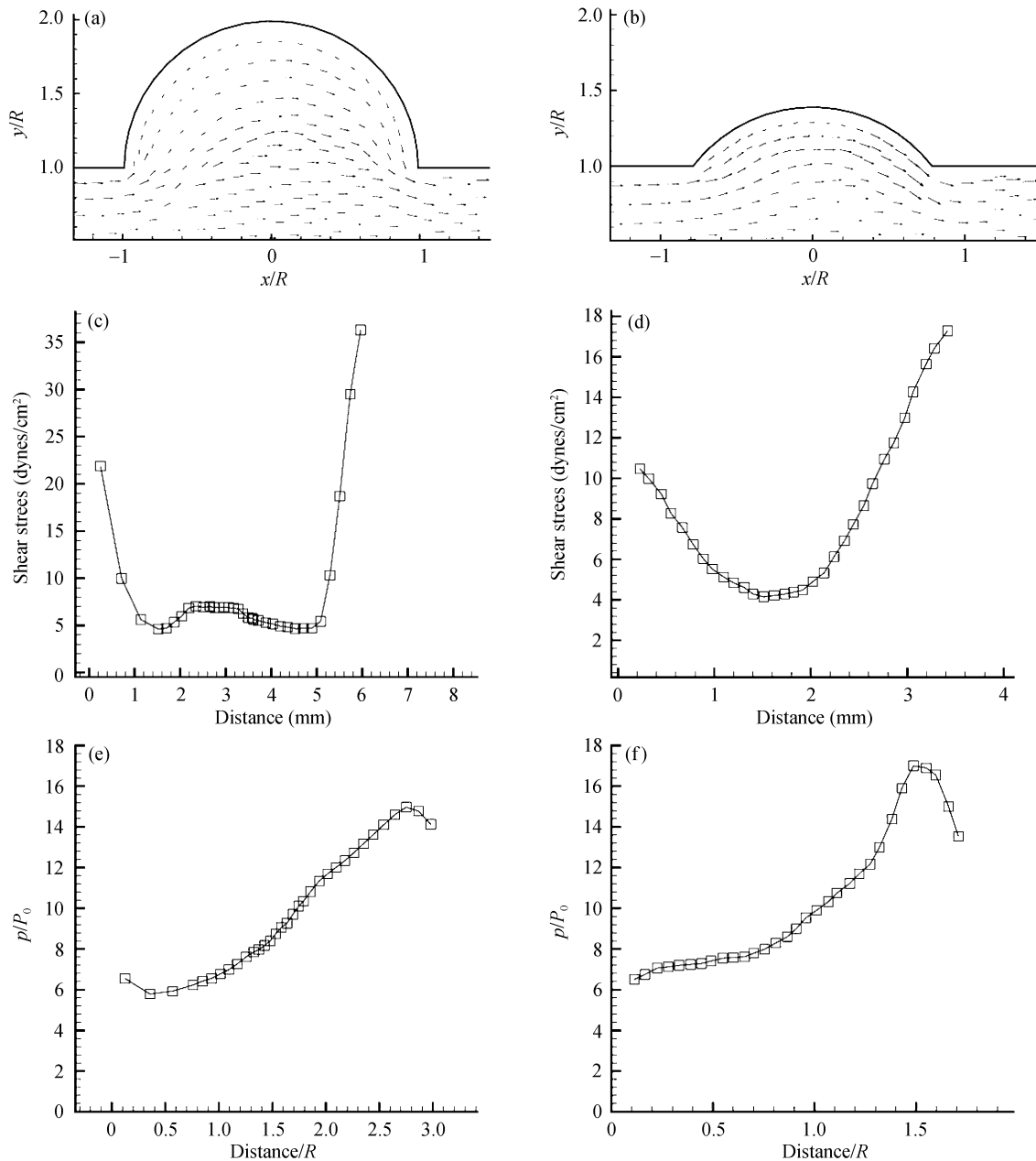


Figure 4 3-D aneurysm. (a) Velocity vector of $z=0$ in Model 1; (b) velocity vector of $z=0$ in Model 2; (c) the shear stress profiles along the wall of aneurysm (Model 1, $z=0$); (d) the shear stress profiles along the wall of aneurysm (Model 2, $z=0$); (e) the pressure profiles along the wall of aneurysm (Model 1, $z=0$); (f) the pressure profiles along the wall of aneurysm (Model 2, $z=0$).

5 Conclusion

Basic Function method is developed to treat the incompressible viscous flow in this paper. By using artificial compressibility, basic function scheme of trigonometric function type is constructed to deal with incompressible viscous flow. We focus our study on the first-order-precision basic function scheme of the trigonometric function type. In comparison with the high-order-precision scheme, the formula of first-order-precision scheme is

simpler with less node number, so the CPU time and memory needed are the least. At first the volume coordinate is adopted for the three-dimensional problem, and the basic function of the first order trigonometric function type and the central and upwind schemes of derivative are established. Then we construct the basic function scheme of the trigonometric function type for solving three-dimensional incompressible Navier-Stokes equations numerically for the first time; in this process

we introduce the artificial compressibility technique, and adopt the technique of flux splitting and the combination of central and upwind schemes.

Flows in finite-length pipe and the hemodynamics in two- and three-dimensional aneurysms are researched numerically by using the basic function of the trigonometric function type and the unstructured grids generation technique. The velocity and pressure distribution of the finite-length pipe calculated by our method agree well with the exact solutions of Poiseuille flow at most regions, some numerical results of two-dimensional an-

eurysms are compared with that of ref. [19] and the agreement is satisfactory. It indicates from the numerical results of aneurysms that the maximal shear stresses and pressures all exhibit in or near the distal region of the aneurysms, and the distal region of the aneurysms is the dangerous region where the aneurysm growth and rupture often happen. Furthermore, the maximal shear stress on the aneurysms wall will increase with increasing aneurysms size, while much improvement should be made in future, such as the pulsatile velocity inflow boundary condition and dense meshes.

- 1 Wu Z N. Fundamental of Computational Fluid Dynamics (in Chinese). Beijing: Science Press, 2001. 130–139
- 2 Orszag S A. Spectral methods for problems in complex geometries. *J Comput Phys*, 1980, 37: 70–92
- 3 Zienkiewicz O C, Taylor R L. The Finite Element Method. 5th ed. Boston: Butterworth-Heinemann, 2000
- 4 Hou H Q, Zhang L, Jin X Z. Finite volume method on unstructured triangular meshes and its applications on convective phenomena. *Chin J Comput Phys*, 2000, 17(4): 381–387
- 5 Shen F. The theoretical research of basic function method in incompressible viscous flow and its applications in aneurysms, and the experimental and theoretical research of Portal hypertension. Doctor Dissertation. Beijing: Peking University, 2004. 1–82
- 6 Lin G. Basic Function method - An innovative numerical method which directly discrete differential operator on unstructured grids. Master Thesis. Beijing: Peking University, 2000. 1–41
- 7 Xie W J. The research and application of basic function method in 3D inviscid compressible flow and unstructured grids generation technique plus remeshing. Master Thesis. Beijing: Peking University, 2002. 1–47
- 8 Li J X. The trigonometric function type basic function method. Master Thesis. Beijing: Peking University, 2003. 1–50
- 9 Chorin A I. A numerical method for solving incompressible viscous flow problem. *J Comput Phys*, 1967, 2: 12–16
- 10 Bowyer A. Computer Dirichlet tessellations. *Comput J*, 1981, 24: 162–166
- 11 Watson D F. Computing the n -dimensional delaunay tessellation with application to voronoi polytopes. *Comput J*, 1981, 24: 167–172
- 12 Jin H, Tanner R I. Generation of unstructured tetrahedral meshes by advancing front technique. *Int J Numer Methods Fluids*, 1993, 36: 1805–1823
- 13 Pirzadeh S. Structured background grids for generation of unstructured grids by advancing front methods. *AIAA J*, 1993, 31: 257–265
- 14 Muller J D, Roe P L, Deconinck H. A frontal approach for internal node generation in delaunay triangulations. *Int J Numer Methods Fluids*, 1993, 17: 241–255
- 15 Wen G B, Chen Z B. Unsteady/Steady numerical simulation of three-dimensional incompressible Navier-Stokes equations on artificial compressibility. *Appl Math Mech*, 2004, 25(1): 53–66
- 16 Rogers S E, Kwak D, Kiri C. Steady and unsteady solution of the incompressible Navier-Stokes equation. 1991, 29(4): 603–610
- 17 Sun S J. The hemodynamical research of cerebral arteriovenous malformation. Doctor Dissertation. Beijing: Peking University, 2002. 1–79
- 18 Wu W Y, Skalak R. The creeping motion in the entry region of a semi-infinite circular cylindrical tube. *Appl Math Mech*, 1983, 4(6): 743–757
- 19 Zhang X W, Yao Z H, Zhang Y, et al. Experimental and computational studies on the flow fields in aortic aneurysms associated with deployment of AAA stent-grafts. *Acta Mech Sin*, 2007, 23: 495–501
- 20 Burleson A C, Strother C M, Turitto V T. Computer modeling of intracranial saccular and lateral aneurysms for the study of their hemodynamics. *Neurosurgery*, 1995, 37(4): 774–784
- 21 Wu W Y. Fluid Mechanics, Vol. 1 (in Chinese). Beijing: Peking University Press. 1982. 205–239
- 22 Fu C J. The 2-D numerical simulation of the hemodynamics related to intracranial aneurysms. Master Thesis. Beijing: Peking University, 2000. 1–40